Bull. Mater. Sci., Vol. 34, No. 4, July 2011, pp. 759–765. © Indian Academy of Sciences.

# Effect of surfactants in synthesis of $CsH_2PO_4$ as protonic conductive membrane

**SORAYA HOSSEINI*, WAN RAMLI WAN DAUD, MARZIEH BADIEI[†] ABDUL AMIR HASSAN KADHUM and ABU BAKAR MOHAMMAD**

Institute of Fuel Cell, [†]Chemical Engineering Process, University Kebangsaan Malaysia, 43600 Bangi, Selangor, Malaysia

MS received 5 October 2009; revised 25 November 2009

**Abstract.** **Cesium dihydrogen phosphate (CDP) powders were synthesized by cetyltrimethylammoniumbromide (CTAB), polyoxyethylene-polyoxypropylene (F-68) and mixture of both surfactants F-68 : CTAB with two molar ratios 0·06 and 0·12 as surfactant solutions at room temperature. The synthesized $CsH_2PO_4$ is characterized by ICP, XRD, TEM, SEM, FT–IR, BET and IS techniques. Based on the width of the (011) XRD diffraction peak and BET measurement, the average size of nanoparticles was ~10 nm in diameter, while the TEM images indicate smaller size than both techniques. The analysis reveals existence of P and Cs with mole ratio 1·02 ± 0·03 which is compatible to molar ratio $CsH_2PO_4$ formula. The experimental results show that the conductivities increase in the order of $CDP_{CTAB} > CDP_{(F\text{-}68\,:\,CTAB)0.12} > CDP_{(F\text{-}68:CTAB)0.06} > CDP_{F\text{-}68}$. The sequence of increasing conductivity is in accordance with the ion exchange capacities of the samples that has direct proportional effect on the proton mobility of samples. Indeed CTAB as cationic surfactant shows the highest proton mobility in the as-obtained samples.**

**Keywords.** **$CsH_2PO_4$; surfactant; nanoparticles; protonic conductivity.**

## 1. Introduction

Extensive research of solid acids shows their utility because of the protonic conductivity properties and useful applications as electrolytes in fuel cells. The chemical composition is $M_aH_b(XO_4)_c$, where M = K, Rb, Cs, $NH_4$; X = S, Se, P and a, b, c are their respective stoichiometric coefficients (Baranov 2003). Cesium dihydrogen phosphate (CDP), or $CsH_2PO_4$, is a member of this group of solid acids, which is built from the discrete $PO_4$ tetrahedral connected by O–H···O hydrogen bonds through the electrostatic interaction of the cesium cation. $CsH_2PO_4$ undergoes a three phase transition; the first is the ferroelectric phase transition at $T$ = 154 K with space group $P2_1$ and completely ordered hydrogen bonds transform. Below this temperature, protons in the shorter hydrogen bond (2·48 Å) are ordered to the oxygen atom of $PO_4$ group, disturbing the $PO_4$ ion configuration and lowering its symmetry (Kennedy and Nelmes 1980; Deguchi *et al* 1982).

At room temperature or paraelectric phase, $CsH_2PO_4$ is monoclinic with space group $P2_1/m$ and two formula units per unit cell ($Z$ = 2) and partly disordered hydrogen bond (JCPDS-ICDD 1995). Morever, it has been reported that $CsH_2PO_4$ undergoes a phase transition at 504 K and space group $Pm3m$ symmetry (cubic) with disordered hydrogen bond which is the 'superprotonic phase transition'. The superprotonic phase transition is distinguished by rapid proton transfer on the hydrogen bonds and the liberation of oxy-anion ($PO_4$) at 504 K (Bronowska 2001; Boysen *et al* 2003; Otomo *et al* 2003). The proton conductivity rises due to superprotonic phase transition from two to three orders of magnitude, reaching values as high as $10^{-2}$–$10^{-3}$ $\Omega^{-1}$ $cm^{-1}$ (Baranov *et al* 1982; Haile *et al* 2001). A study was undertaken to investigate the CDP morphology, using methanol and polyols by Kim *et al* (2006) which showed that samples with spherical morphology and smaller particle size produce relatively higher values of conductivity. The synthesis of CDP employs various methods such as solvent evaporation and the addition of a second solvent to reduce the solubility of the solute. A new method for the preparation of CDP is the surfactants method with reduction in particles size. In this paper, the surfactants method is used to synthesize $CsH_2PO_4$ nanoparticles by cationic surfactant as CTAB, non-ionic surfactant F-68 and the surfactants mixture (F-68:CTAB) with two molar ratios 0·06 and 0·12. The micelle concentration of CTAB determines the shape of the nanoparticles. CTAB can generate different morphology using concentrations above and below critical micelle concentration (CMC). It forms spherical micelles above the CMC (0·00001 mole in solvent) and produces rod shape micelles below the CMC (Olivera *et al* 2006; Jun and Ki 2009). The conductivity also depends

*Author for correspondence (soraya@eng.ukm.my)

on the morphology and degree of crystallinity (McCall *et al* 1989).

## 2. Experimental

The synthesis of $CsH_2PO_4$ nanoparticles was achieved using a stoichiometric amount of cesium carbonate $Cs_2CO_3$ (99·99% Aldrich), orthophosphoric acid $H_3PO_4$ (85%wt Aldrich) and two surfactants Cetyltrimethylammonium-bromide (99% SIGMA), polyoxyethelen-polyoxypropylene (Pluronic, F-68 SIGMA) and a mixture of both surfactants (F-68:CATB) with two molar ratios 0.06 and 0·12. The reaction is follows:

$$Cs_2CO_3 + 2H_3PO_4 \rightarrow 2CsH_2PO_4 + CO_2 + H_2O.$$

Samples of different sized nanaoparticle were prepared with CTAB, F-68 (F-68: CTAB)$_{0·06}$ and (F-68: CTAB)$_{0·012}$. For CDP preparation, measured amount of $Cs_2CO_3$ was dissolved in distilled water. The surfactant solution was separately prepared using CTAB, F-68 (F-68: CTAB)$_{0·06}$, (F-68: CTAB)$_{0·12}$ and ethanol (99·99%) with vigorous stirring (figure 1). After 20 min, when all the surfactants have dissolved in ethanol, the solution becomes clear and then it was added to the $Cs_2CO_3$ aqueous solution with continuous stirring at room temperature for 10 min. A measured amount of $H_3PO_4$ was added, drop-wise, into the resulting solution under stirring for 1 h. Subsequently, a white precipitate of $CsH_2PO_4$ powder is formed. The as-prepared sample was dried at 130°C overnight and then collected as dry powder. The first endothermic peak of nanoparticles was observed, by DSC and TGA analyses in the range of 233–244°C with weight loss of more than 3% (Hosseini *et al* 2009). For this reason and to prevent side productions of $CsH_2P_2O_7$ and $CsPO_3$, after sufficient drying, the white precipitate was calcinated at 220°C for 8 h under $N_2$ gas. Impedance was measured using a Solarton 200 over the frequency range 0·01 Hz–1 MHz, a controller of temperature West Model 6100, a furnace with standard thermocouple °C under Ar/$H_2O$ (Ar: $H_2O$ = 0.9 : 0·1). The samples were pressed under a pressure of 191 kg cm$^{-2}$ to form pellets of diameter and thickness, 10 mm and 2 mm respectively. Both sides of the pellets were coated with carbon paste using graphite. The pellet was sandwiched between two silver holders and connected to impedance analyzer. The real $Z'$ and the imaginary $Z''$ parts of the impedance were measured between 30 and 260°C for intervals of 20°C. Data was analysed using commercial software package, ZView2 to calculate the proton conductivity.

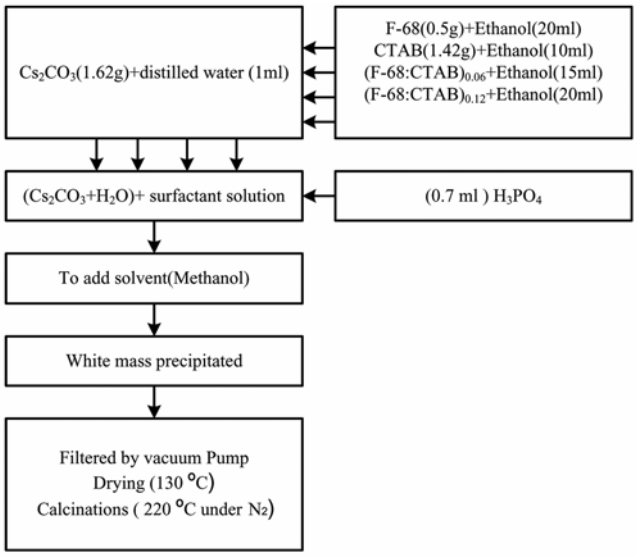


**Figure 1.** Flow chart for the synthesis of $CsH_2PO_4$ nanoparticles by the surfactants.

## 3. Analytical instruments

Particle structure was identified using a diffractometer (Bruker D8 Advance) with Cu$K\alpha_1$ radiation. The particle size and conglomeration state were recorded using transmission electron microscopy (Philips CM-12) at an accelerating voltage of 20 kV. The aggregates of CDP were rinsed several times with 95% ethanol. After employing ultrasonic on the samples for 5 min at 20°C, the suspension was dripped onto a small cupper grid and air-dried for measuring the size. Scanning electron microscopy (SEM) was carried out on an electron microscope system (LEO 1450VP) attached to EDX analyzer. IR spectrum was recorded on FT–IR spectrophotometer (Nicolet 6700) in the range of 400–4000 cm$^{-1}$. Sample was prepared by finely dispersing powder material on a KBr carrier. The specific surface area of the calcined powders was measured by BET analysis (Ami 2000) using $N_2$ in a three step adsorption-desorption process. Proton conductivity was measured by impedance spectroscopy technique, using a Solarton 200 over the frequency range 0·01 Hz–1 MHz, in the temperature range of 30–260°C.

## 4. Results and discussion

Nucleation and the growth mechanism strongly influence particle morphology. The presence of impurities, especially macromolecular impurities such as polymers (Manna *et al* 2000) or surfactants can alter the shape of the growing crystal. In view of this, surfactants CTAB, F-68 and mixture of F-68: CTAB were used to yield smaller particles and different particle morphology.

### 4.1 *ICP and XRD analysis*

$CsH_2PO_4$ nanoparticles were prepared as discussed in the experimental section. Different sizes of nanoparticles were obtained by changing surfactant type and the molar concentration of (F-68: CTAB) solution.

In order to evaluate the mole ratio Cs/P of the samples, analysis of elements was carried out in the five the samples. The values of P and Cs are reported for both the group of samples (using surfactant and without surfactant). Clearly, the value of

$$\frac{\mu g\ (\text{component})}{g(CsH_2PO_4)},$$

in the sample (without surfactant) is more than the other samples. This difference is due to the calcination process during the removal of the template (due to surfactants) around the particle by heat. The calcination process results in the loss of some P and Cs in these compounds. The mole ratio of Cs/P is 1·02 ± 0·03 which is compatible to the mole ratio of $CsH_2PO_4$ formula.

The structures of different sizes of nanoparticles namely $CDP_{CTAB}$, $CDP_{F\text{-}68}$, $CDP_{(F\text{-}68:\ CTAB)0\cdot06}$, $CDP_{(F\text{-}68:\ CTAB)0\cdot12}$ were studied at room temperature using X-ray diffraction which were measured in the $2\cdot3° \le \theta \le 60°$ range on a Bruker AXS D8 Advance device operated at 40 kV, 40 mA with CuK$\alpha$ radiation ($\lambda$ = 1·5405 Å) at step size of $2\theta$ = 0.02° and a fixed counting time of 1 s/step and analyzed with a EVA software. Cell parameters were determined by least-squares of all reflections in the measured $2\theta$ range as listed in table 1. The refinement leads to rather good agreement between the experimental and calculated XRD patterns and yields acceptable reliability factors: $R$, $R_{exp}$, $R_{wp}$ and GOF (Rietveld 1969; Larson and Von Dreele 2000; Kojitani *et al* 2005). In Rietveld analysis, a least squares method is used to obtain the best possible fit between the observed and simulated powder diffraction patterns. Residual of fitting ($I_o - I_c$) between observed ($I_o$) and calculated ($I_c$) intensities of each fitting is plotted under respective patterns as shown in figure 2. The fitting quality is relatively good and varies between 1·02 and 1·7.

All the diffraction peaks in figures 2a, b, d, e index well to the monoclinic phase structure of $CsH_2PO_4$ (JCPDS 01-084-0122) (Matsunaga *et al* 1980). All the diffraction peaks in figure 2c index well to the orthorhombic phase structure of $CsH_2PO_4$ (JCPDS 01-083-2191) (Rashkovich 1991). The maximum peak located at 24·5° corresponds to the (011) plane with the other principal peaks corresponding to the planes (110), (001), (020), (021) and (220) located at 17°, 19°, 30°, 34·5° and 38°, respectively. Nanoparticle sizes were calculated based on the half-peak width of the diffraction peak at miller index (011, $2\theta$ = 24·5°) using the Scherrer's equation. The average crystallite diameter, $d$, was estimated from the broadening of the XRD peak widths by the Scherrer formula

$$D = \frac{K\lambda}{\beta\cos\theta}, \qquad (1)$$

where $\lambda$ is the wavelength of the radiation, $\beta$ is the integral width of the Bragg reflection at $2\theta$, and $K$ is the Scherrer constant (0·93) which depends on factors such as the geometry of the crystallites (Burton *et al* 2009). Figure 2 shows XRD patterns for the CDP samples prepared with and without surfactants. The peaks in the $CDP_{evaporation}$ pattern were noticeably sharper, indicating larger, more crystalline particles than in the $CDP_{surfactant}$.

Miller index for the observed peaks are given figure 2e, wherein some differences are noticed in the Miller indexes for samples that directly influence morphology of the particles. The growth and morphology of crystals depend on Miller index planes. The effect of methanol solution on crystal morphology suppresses crystal growth by extracting solvent water from solution and adsorbing onto the crystal surface; adsorption on to particular sites of crystallites change the expanded capacity of every plane (Dongli *et al* 2005). EDX analyses showed no impurity yield during synthesis.

### 4.2 *BET and TEM analysis*

The specific surface area of samples was characterized by $N_2$ adsorption at liquid nitrogen temperature using an Ami 2000 instrument. Prior to analysis, the samples were placed in vacuum at 200°C for 2 h to remove the surface adsorbed species. The data were analysed according to

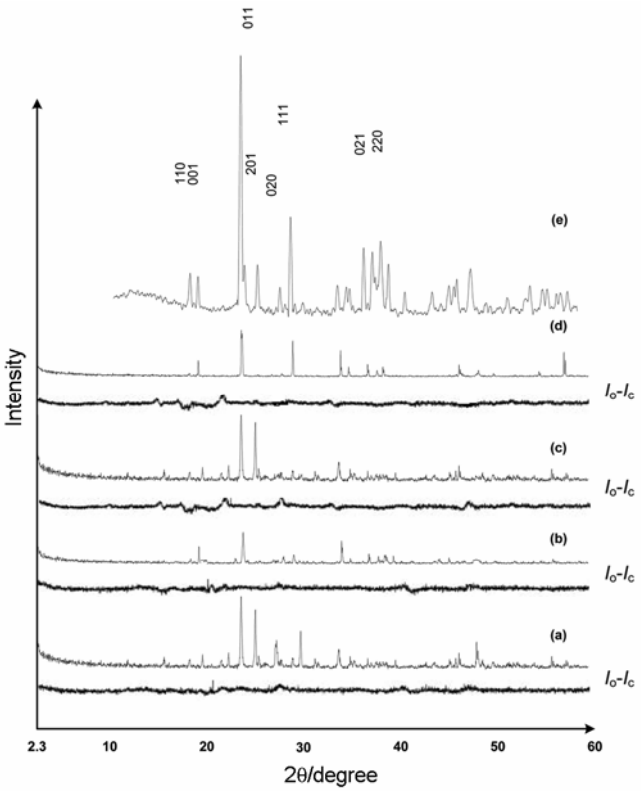


**Figure 2.** XRD patterns of the powder CDP, using (a) $CDP_{CTAB}$, (b) $CDP_{F\text{-}68}$, (c) $CDP_{(F\text{-}68:CTAB)0\cdot06}$, (d) $CDP_{(F\text{-}68:CTAB)0\cdot12}$ and (e) CDP (without surfactant).

**Table 1.** Structural parameters of the CDP samples at room temperature.

| Parameters | $CDP_{[17]}$ | $CDP_{F\text{-}68}$ | $CDP_{(F\text{-}68:CTAB)0\cdot06}$ | $CDP_{(F\text{-}68:CTAB)0\cdot12}$ | $CDP_{CTAB}$ |
|---|---|---|---|---|---|
| $\alpha$ | 7·912 | 7·997 | 4·872 | 7·995 | 7·907 |
| $b$ | 6·386 | 6·383 | 6·368 | 6·382 | 6·386 |
| $c$ | 4·88 | 4·88 | 15·049 | 4·88 | 4·88 |
| $\beta$ | 107·73 | 107·73 | 90·22 | 107·75 | 107·71 |
| $z$ | 2 | 4 | 4 | 2 | 2 |
| space | $P2_1/m$ | $C2/c$ | $B2_1/m$ | $P2_1/m$ | $P2_1/m$ |
| GOF | | 1·105 | 1·127 | 1·153 | 1·165 |
| $R$ | | 4·35% | 5·32% | 6·12% | 5·15% |
| $R_{wp}$ | | 7·94% | 9·22% | 8·29% | 8·34% |
| $R_{exp}$ | | 6·08% | 7·54% | 7·34% | 6·17% |

the Brunauer–Emmet–Teller (BET) analysis based on the Langmuir equation. The average particle size can be estimated by assuming that all particles have the same shape and size. The average particle diameter, $D$, is given by (Hammes *et al* 2008)

$$D = \frac{6}{S_{sp}.\rho_p}, \tag{2}$$

where $S_{sp}$ and $\rho_P$ are the specific surface area per unit mass of the sample and the true density, respectively. The nanoparticle density was calculated by pycnometer using dimethylformamide (DMF) as listed in table 2.

Figure 3 shows the TEM micrograph of $CDP_{(F\text{-}68:\ CTAB)0\cdot06}$. The particle size is determined by transmission electron microscope (TEM) images that are based on an automated image analysis. The normal size distribution of the particles calculated by mathematical equations comprising of the parameters, mean ($\zeta$), standard deviation ($\nu$) and nanoparticle size ($x$) is as follows:

$$F(x) = \frac{e^{\frac{-(x-\zeta)^2}{2\nu^2}}}{\sqrt{2\pi\nu^2}}, \tag{3}$$

According to TEM analysis and the normal size distribution plots, the smallest size of particles is generated by surfactant F-68 as shown in table 2. It is usual the TEM analysis to yield average particle sizes biased toward smaller sizes, since the method of sample preparation often uses a TEM grid which selects (filters) only the smallest particles deposited from solution, then two methods of particle size measurement was performed by XRD and BET measurement. The comparison between these techniques is listed in table 2. The obtained particle sizes from the XRD were in the range 10 nm, in good agreement with those calculated from BET analysis.

### 4.3 *IS and FTIR analysis*

The protonic conductivity of $CsH_2PO_4$ nanoparticles is performed by electrochemical impedance spectroscopy technique in the frequency range 0·01 Hz to 1 MHz for samples $CDP_{F\text{-}68}$, $CDP_{CTAB}$, $CDP_{(F\text{-}68:CTAB)0\cdot06}$ and $CDP_{(F\text{-}68:CTAB)0\cdot12}$. The impedance spectroscopy of $CsH_2PO_4$ nanoparticles are represented in Nyquist diagram in rang of temperature 30–260°C. Typical impedance spectra were obtained below superprotonic phase (210°C), at superprotonic phase (230°C) and above superprotonic phase (260°C). Good agreement was observed between the experimental and the equivalent circuits (using Zview2) (Hosseini *et al* 2011). The relative error between the experimental and calculated spectra is less than 3%. Due to the change in relative contribution of bulk electrolyte and interface to the total impedance, the spectra changed remarkably below and above the superprotonic transition temperature as shown in figure 4.

Temperature dependencies of the protonic conductivity obtained using impedance measurement data by the classical Arrhenius equation are presented in figure 5.

$$\sigma = \frac{A}{R}\exp\left(\frac{-E}{KT}\right), \tag{4}$$

The Arrhenius plot consists of two straight lines of different slopes at the regions of low and high temperatures, respectively. The shape of the plot has been generally attributed to the existence of distinct mechanisms, involving of two different activation energies, each one dominating at a particular range of temperatures. $CsH_2PO_4$ undergoes a thermal decomposition at 149°C which, much like the transition at 230°C, gives rise to an increase in conductivity (Ortiz *et al* 1999a, b). The non-linearity of Arrhenius plot resulted due to the different thermal behaviors of $CsH_2PO_4$ and the different activation energies.

The conductivities of the monoclinic phases increase sharply at the superprotonic transition temperatures, which coincide with the thermal events observed by DSC analysis. The impedance analysis indicate increasing conductivity as sequential $CDP_{CTAB} > CDP_{(F\text{-}68:\ CTAB)0\cdot012} > CDP_{(F\text{-}68:CTAB)0\cdot06} > CDP_{F\text{-}68}$. As seen in figure 5, the maximum jump in protonic conductivity is noticed in the range 210–230°C wherein upon heating above 230°C, the protonic conductivity decrease in samples

**Table 2.** Average particle size, ion exchange capacity and density of nanoparticles.

| Samples | TEM (nm) | XRD (nm) | BET (nm) | Ion exchange capacity (mmol $g^{-1}$) | Density (g $cm^{-3}$) |
|---|---|---|---|---|---|
| $CDP_{CTAB}$ | 3·7 ± 0·488 | 10·3 ± 0·45 | 11·35 ± 0·48 | 1·09 ± 0·02 | 3·53 ± 0·13 |
| $CDP_{F\text{-}68}$ | 2·66 ± 0·89 | 6·85 ± 0·87 | 8·71 ± 0·69 | 0·75 ± 0·03 | 3·42 ± 0·2 |
| CDP (F-68:CTAB)$_{0·06}$ | 3·5 ± 0·56 | 11·23 ± 0·54 | 10·81 ± 0·45 | 0·89 ± 0·02 | 3·37 ± 0·18 |
| CDP (F-68:CTAB)$_{0·12}$ | 4·89 ± 0·27 | 12·37 ± 0·69 | 11·88 ± 0·21 | 0·91 ± 0·04 | 3·49 ± 0·11 |

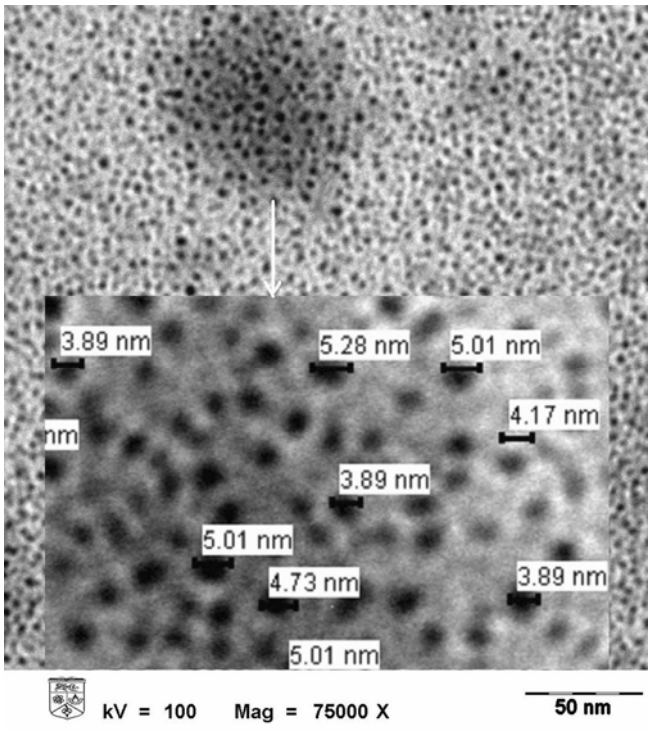


**Figure 3.** TEM patterns of $CDP_{(F\text{-}68:CTAB)0·06}$.

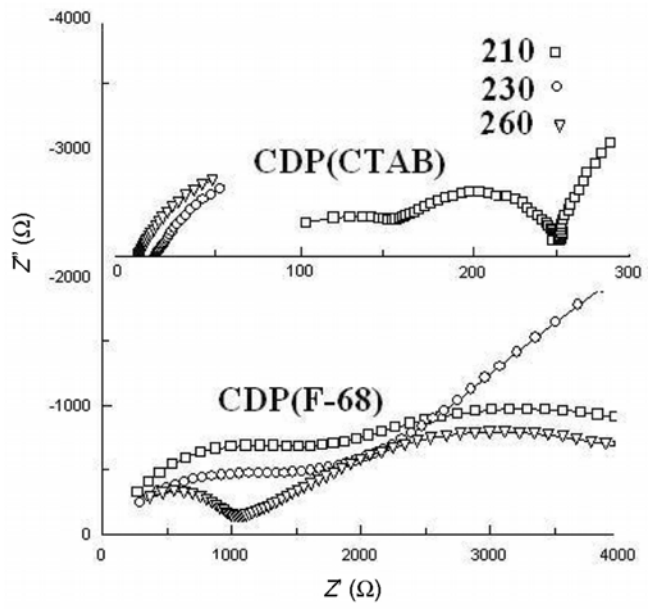


**Figure 4.** Nyquist plots of two samples $CDP_{CTAB}$ and $CDP_{(F\text{-}68:CTAB)0·06}$.

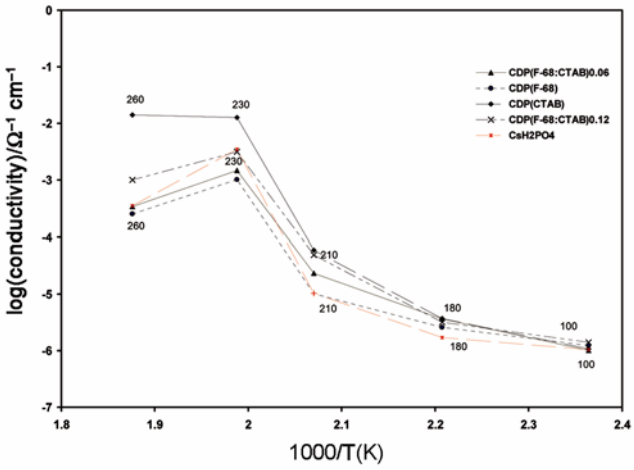


**Figure 5.** A comparative temperature dependence of the conductivity CDP samples.

$CDP_{(F\text{-}68:CTAB)0·012}$, $CDP_{(F\text{-}68:CTAB)0·06}$ and $CDP_{F\text{-}68}$ except in $CDP_{CTAB}$ where there is a slight increase above the phase transition temperature. Proton conductivities of the nanparticles are consistent with their ion exchange capacity (IEC) values, and are well represented by Arrhenius equation (Daiko *et al* 2007). Among the CDP samples, CDPCTAB showed the highest IEC value. This shows the direct proportional effect of IEC on the proton mobility.

Solid acids show high protonic conductivity at superprotonic phase transition accompanied by breaking of the hydrogen bonds, due to the rotational motion of $XO_4$ tetrahedrons. In order to confirm the presence of hydrogen bonds and anions $PO_4^{-3}$ in the crystal lattice, infrared absorption spectra of the samples was taken in the range of 4000–400 $cm^{-1}$, as shown in figure 6. The bands were assigned to the paraelectric phase of $CsH_2PO_4$ nanoparticles (stable at room temperature). The IR spectrum consists of a number of well separated groups of bands; 3600–1300 $cm^{-1}$ (high frequency H modes), 1300–800 $cm^{-1}$ (stretching P–O and bending P–OH modes) and 800–400 $cm^{-1}$ (stretching OPO modes and Cs…O) (Le Calve *et al* 1989; Romain and Novak 1991; Hubert *et al* 1995). The ABC structure of the $\nu$(OH) stretching vibrations is observed for many solid acids where the stretching OH…O hydrogen bonds reveal centers of lines at 2800, 2500 and 1650 $cm^{-1}$ (Kalevitchayb *et al* 1995). For each OH bond, the O–H motions are known as $\nu$ (OH), $\delta$ (OH) and $\gamma$ (OH) i.e. stretching O–H, in plane

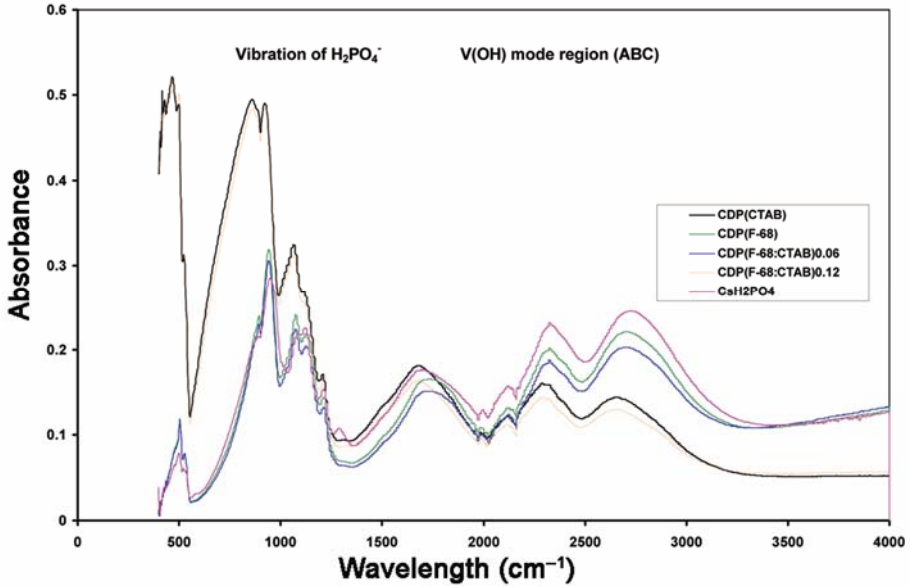


**Figure 6.** IR spectra of the samples CDP at ambient temperature (400–4000 $cm^{-1}$).

and out-of-plane bending P–O–H vibration, respectively (Koleva *et al* 2009). Due to the Fermi resonance between $\nu$ (OH) and overtones of the deformation modes $\delta$ (OH) and $\gamma$ (OH) appear as the ABC structure. The phenomenon was noticed in some solid acids that can be compatible with the ABC structure (Toupry and Poulet 1981; Kalevich *et al* 1993). The well separated peaks of CDP nanoparticles at 2650, 2300 and 1650 $cm^{-1}$ in the IR spectra can be assigned to the ABC bonds of OH. The strong absorption of the samples in the region 900–1200 $cm^{-1}$ in the IR spectra can undoubtedly be assigned to the components of the $PO_4$ while the four bands at 1185, 1140, 1070 an 940 $cm^{-1}$ are attributed to the P–O stretching modes in the $H_2PO_4$ – anion that is compatible to reported data (Koleva *et al* 2009). The generated bond due to Cs…O–H is observed at 490 $cm^{-1}$. According to Beer's law measured absorbance shows a linear relationship with concentration of impurity, absorptivity of a particular bond and thickness of sample (Ross Boyle 2005). The increase in absorbance values of samples $CDP_{CTAB}$ and $CDP_{(F\text{-}68:CATB)0\cdot12}$ can be due to the impurity concentration.

## 5. Conclusions

It is possible to produce $CsH_2PO_4$ nanoparticles of different sizes using the chemical method by surfactants. The XRD, TEM and BET data were obtained to confirm nanosize of these materials. It is also observed that the particle size depends on molar concentration of the surfactant solution and type of surfactant. The measured proton conductivity indicates the increasing as sequential $CDP_{CTAB}$ > $CDP_{(F\text{-}68:CTAB)0\cdot012}$ > $CDP_{(F\text{-}68:CTAB)0.06}$ > $CDP_{F\text{-}68}$ respectively. Among the samples, $CDP_{CTAB}$ had the highest value of proton mobility.

## Acknowledgement

The authors appreciate the financial support of the IRPA-02-02-02-0006 PR0023/11-08.

## References

Baranov A I 2003 *Cryst. Rep.* **46** 1012

Baranov A I, Shuvalov L A and Shchagina N M 1982 *JETP Lett.* **36** 459

Boysen D A, Haile S M, Liu H and Secco R A 2003 *Chem. Mat.* **15** 727

Bronowska W 2001 *J. Chem. Phys.* **114** 611

Burton A W, Ong K, Rea Th and Chan I Y 2009 *Micro. Meso. Mat.* **117** 75

Daiko Y, Katagiri K, Ogura K, Sakai M and Matsuda A 2007 *Solid State Ionic* **178** 601

Deguchi K, Nakamura E and Okaue E 1982 *J Phys. Soc.* **51** 3569

Dongli Xu, Dongfeng X and Henryk R 2005 *J. Mol. Struct.* **740** 37

Jun Y and Ki Zh 2009 *Technology Application* DOI CNKI:SUN:HCSY.0.2009-03-009

Haile S A, Boysen D A, Chisholm C R I and Merie R B 2001 *Nature* **410** 910

Hammes K, Smernik R J, Skjemstad J O and Schmidtt W 2008 *Appl. Geoch.* **23** 2113

Hosseini S, Mohamad A B, Khadum A H and Wan Doud W R 2009 *J. Therm. Anal. Cal.* Doi: 10.1007/s10973-009-0132-2

Hosseini S, Homaeei M, Mohamad A B, Malekbala M R and Khadhum A A H 2011 *Phys. B: Condens. Matter* **406** 1689

Hubert J, Jayakumar V S and Aruldhas G 1995 *J. Solid State Chem.* **120** 343
JCPDS-ICDD 1995 *Database* **35** 746
Kalevich N I, Maljarevich A M and Posledovich M R 1993 *Bull. Russ. Chem. Phys.* **12** 1015
Kalevich N I, Posledovich M R and Rodin S V 1993 *Bull. Russ. Acad. Sci. Phys.* **57** 385
Kalevitchayb N I, Arnscheidtb B, Pelzlb J and Rodina S V 1995 *J. Mol. Struct.* **348** 361
Kennedy N S J and Nelmes R J 1980 *J. Phys.* **C13** 4841
Kim J, Ahn Y S, Ruth M I and Park C W 2006 *J. Power Sources* **163** 107
Kojitani H, Kido M and Akaogi M 2005 *Phys. Chem. Miner.* **32** 290
Koleva V, Stefov V, Cahil A, Najdoski M, Šoptrajanov B, Engelen B and Lutz H D 2009 *J. Mol. Struct.* **917** 117
Larson A C and Von Dreele R B 2000 Los Alamos National Laboratory Report LAUR 86-748, USA
Larson A C and Von Dreele R B 2006 *General structure analysis system technical manual LANSCE*, MS-H805 2000 (LAUR: Los Almos National University) **Vol. 86** p. 66
Le Calve N, Romain F, Limage M H and Novak A 1989 *J. Mol. Struct.* **200** 131
Manna L, Scher E C and Alvisatos A P 2000 *J. Am. Chem. Soc.* **122** 12700
Matsunaga H, Itoh K and Nakamura E 1980 *J. Phys. Soc. Jpn.* **48** 2011
McCall R P, Ginder J M, Roe M G, Asturias G E, Scherr E M, Macdiarmid A G and Epstein A J 1989 *Phys. Rev.* **B39** 10174
Olivera C, Jankovicb I, Comorb M and Vladimirova S 2006 *J. Collo. Inter. Sci.* **301** 692
Ortiz E, Vargas R and Mellander B 1999a *J. Chem. Phys.* **110** 4847
Ortiz E, Vargas R and Mellander B 1999b *Solid State Ionics* **125** 177
Otomo J, Minagawa N, Wen C, Eguchi K and Takahashi H 2003 *Solid State Ionic* **156** 357
Rashkovich L N 1991 KDP-family single crystals (IOP Publishing)
Rietveld H M 1969 *Acta Crystall.* **2** 65
Romain F and Novak A 1991 *J. Mol. Struct.* **263** 69
Ross Boyle 2005 *Thermo fisher scientific* (Madison WI, USA)
Toupry N and Poulet H 1981 *Postollec MLe J Raman Spect.* **11** 81